Mon. Not. R. Astron. Soc. **399,** 683–698 (2009) doi:10.1111/j.1365-2966.2009.15338.x

The 6dF Galaxy Survey: final redshift release (DR3) and southern large-scale structures

D. Heath Jones,[1⋆] Mike A. Read,[2] Will Saunders,[1] Matthew Colless,[1] Tom Jarrett,[3] Quentin A. Parker,[1,4] Anthony P. Fairall,[5]† Thomas Mauch,[6] Elaine M. Sadler,[7] Fred G. Watson,[1] Donna Burton,[1] Lachlan A. Campbell,[1,8] Paul Cass,[1] Scott M. Croom,[7] John Dawe,[1]† Kristin Fiegert,[1] Leela Frankcombe,[8] Malcolm Hartley,[1] John Huchra,[9] Dionne James,[1] Emma Kirby,[8] Ofer Lahav,[10] John Lucey,[11] Gary A. Mamon,[12,13] Lesa Moore,[7] Bruce A. Peterson,[8] Sayuri Prior,[8] Dominique Proust,[13] Ken Russell,[1] Vicky Safouris,[8] Ken-ichi Wakamatsu,[14] Eduard Westra[8] and Mary Williams[8]

[1]*Anglo-Australian Observatory, PO Box 296, Epping, NSW 1710, Australia*
[2]*Institute for Astronomy, Royal Observatory, Blackford Hill, Edinburgh EH9 3HJ*
[3]*Infrared Processing and Analysis Center, California Institute of Technology, Mail Code 100-22, Pasadena, CA 91125, USA*
[4]*Department of Physics, Macquarie University, Sydney 2109, Australia*
[5]*Department of Astronomy, University of Cape Town, Private Bag, Rondebosch 7700, South Africa*
[6]*Astrophysics, Department of Physics, University of Oxford, Keble Road, Oxford OX1 3RH*
[7]*School of Physics, University of Sydney, NSW 2006, Australia*
[8]*Research School of Astronomy & Astrophysics, The Australian National University, Weston Creek, ACT 2611, Australia*
[9]*Harvard-Smithsonian Center for Astrophysics, 60 Garden St MS20, Cambridge, MA 02138-1516, USA*
[10]*Department of Physics and Astronomy, University College London, Gower St, London WC1E 6BT*
[11]*Department of Physics, University of Durham, South Road, Durham DH1 3LE*
[12]*Institut d'Astrophysique de Paris (CNRS UMR 7095), 98 bis Bd Arago, F-75014 Paris, France*
[13]*GEPI (CNRS UMR 8111), Observatoire de Paris, F-92195 Meudon, France*
[14]*Faculty of Engineering, Gifu University, Gifu 501-1193, Japan*

Accepted 2009 June 30. Received 2009 June 27; in original form 2009 March 31

ABSTRACT

We report the final redshift release of the 6dF Galaxy Survey (6dFGS), a combined redshift and peculiar velocity survey over the southern sky ($|b| > 10^{\circ}$). Its 136 304 spectra have yielded 110 256 new extragalactic redshifts and a new catalogue of 125 071 galaxies making near-complete samples with (K, H, J, $r_{\rm F}$, $b_{\rm J}$) $\leq$ (12.65, 12.95, 13.75, 15.60, 16.75). The median redshift of the survey is 0.053. Survey data, including images, spectra, photometry and redshifts, are available through an online data base. We describe changes to the information in the data base since earlier interim data releases. Future releases will include velocity dispersions, distances and peculiar velocities for the brightest early-type galaxies, comprising about 10 per cent of the sample. Here we provide redshift maps of the southern local Universe with $z \leq 0.1$, showing nearby large-scale structures in hitherto unseen detail. A number of regions known previously to have a paucity of galaxies are confirmed as significantly underdense regions. The URL of the 6dFGS data base is http://www-wfau.roe.ac.uk/6dFGS.

Key words: surveys – galaxies: distances and redshifts – cosmology: observations – large-scale structure of Universe.

1 INTRODUCTION

The advent of wide-field multiplexing spectrographs over the past decade has produced huge advances in our knowledge of the structure and content of the low-redshift universe. Surveys such as the 2dF Galaxy Redshift Survey (2dFGRS; Colless et al. 2001) and the

⋆E-mail: heath@aao.gov.au
†Deceased.

Sloan Digital Sky Survey (SDSS; York et al. 2000; Abazajian et al. 2009) have characterized the luminosity and clustering properties of galaxies in unprecedented detail. On their own, large-scale redshift surveys can be used to map the galaxy power spectrum and redshift-space distortions resulting from the underlying distribution of mass (e.g. Peacock et al. 2001; Percival et al. 2001). The measurement of related clustering parameters such as bias (b) and mass density (Ω) has allowed these surveys to constrain the amount and distribution of dark matter to unprecedented precision. Redshift surveys have also placed tight constraints on Λ cold dark matter models of the Universe (e.g. Spergel et al. 2007) when combined with the results of supernovae distance measurements (Riess et al. 1998; Schmidt et al. 1998; Perlmutter et al. 1999) and the cosmic microwave background (Bennett et al. 2003). Within this context, the focus has shifted towards an improved understanding of galaxy mass assembly and structure formation generally (e.g. Baugh 2006). A combined redshift and peculiar velocity survey, with dynamical measures of galaxy masses and large-scale motions, offers even better constraints on parameters of cosmological interest than a survey of redshifts alone (Burkey & Taylor 2004; Zaroubi & Branchini 2005).

The 6dF Galaxy Survey[1] (6dFGS; Jones et al. 2004, 2005) is a near-infrared (NIR) and optically selected redshift and peculiar velocity survey. The K sample is the primary 6dFGS target selection and is complete to $K = 12.65$.[2] Targets were added to make secondary samples in J, H, $b_{\rm J}$ and $r_{\rm F}$ complete to 12.95, 13.75, 15.60 and 16.75, respectively. A number of smaller samples, selected from various catalogues and wavelengths, fill out the target allocations.

The NIR magnitudes are total extrapolated magnitudes taken from the 2MASS Extended Source Catalog (XSC; Jarrett et al. 2000). NIR selection is advantageous because it closely tracks the older stellar populations that dominate the stellar mass in galaxies. Furthermore, extinction (both internal and Galactic) is greatly lessened and stellar mass-to-light ratios are more tightly defined (Bell & de Jong 2001). The $b_{\rm J}$ and $r_{\rm F}$ photometry comes from the SuperCOSMOS catalogue (Hambly et al. 2001a,b), following its recalibration for the 2dFGRS (Cole et al. 2005). The peculiar velocity survey uses velocity dispersions and photometric scalelengths to derive dynamical masses and Fundamental Plane distances and peculiar velocities for a subset of more than 10 000 bright, early-type galaxies (Campbell 2009).

The 6dFGS magnitude limits are $\sim$1.5 mag brighter than the magnitudes at which incompleteness starts to affect the 2MASS XSC ($K \lesssim 14$). Examination of the bivariate distribution of surface brightness and galaxy luminosity for the entire 6dFGS sample (Jones et al., in preparation) shows sample selection to be robust against surface brightness selection effects (see e.g. Bell et al. 2003; McIntosh et al. 2006). The limiting isophote at which 6dFGS magnitudes were measured ($\mu_K = 20\,{\rm mag\,arcsec^{-2}}$) is brighter than the values at which 2MASS was found to be incomplete by Bell et al. and McIntosh et al.

The 6dFGS has thus far been used in studies of large-scale structure (e.g. Fleenor et al. 2005, 2006; Proust et al. 2006; Radburn-Smith et al. 2006; Boué et al. 2008), luminosity and stellar mass functions (Jones et al. 2006, in preparation), the influence of local density and velocity distributions (Erdogdu et al. 2006a,b), among others. The Early and First Data Releases (DR1; see below) alone yielded new redshifts for 277 ACO (Abell, Corwin & Olowin) clusters ($z \lesssim 0.1$) without previous redshifts (Andernach et al. 2005), and the full data have yielded more than 400. Examples of the full three-dimensional (3D) space structure of the 6dFGS can be seen in Fluke, Barnes & Jones (2009). The 6dFGS has also been used to study special interest samples selected for their luminosity at X-ray and radio wavelengths (Mauch & Sadler 2007; Mauduit & Mamon 2007; Sadler et al. 2007). Future surveys with next generation radio telescopes such as Australian Square Kilometre Array Pathfinder (ASKAP) and the Square Kilometre Array (SKA) (e.g. Blake et al. 2004; van Driel 2005; Rawlings 2006) will also benefit from the legacy of 6dFGS, as they probe comparable volumes in H I with the benefit of prior redshift information across most of the southern sky.

This paper describes the final data release of 6dFGS redshifts. Earlier incremental data releases in 2002 December, 2004 March and 2005 May have made the first 90k redshifts publicly available through an online data base. In Section 2 we give an overview of the 6dFGS including the characteristics and scope of the data set. Section 3 describes the final instalment as well as its access through our online data base. Details of changes and additions superceding earlier releases are also given. In Section 4 we present redshift maps of the southern sky in both equatorial and Galactic coordinate projections, and discuss major large-scale structures. Concluding remarks are made in Section 5.

2 SURVEY OVERVIEW

2.1 Background

The primary references for detailed information about the 6dFGS are Jones et al. (2004) and this paper. The former describes target selection and field allocations, the 6dF instrument and data reduction and redshifting methodology. It also characterizes the DR1 (46k redshifts) and the online data base. Jones et al. (2005) describe the Second Data Release (DR2; 83k redshifts) and discuss a number of small changes to the data. Earlier papers describe the 6dF instrument (Parker, Watson & Miziarski 1998; Watson et al. 2000) and the field placement algorithm used to optimize target coverage (Campbell, Saunders & Colless 2004). Data base users are encouraged to consult these and other papers on the 6dFGS publications web page.[3] This paper marks the final public data release of 6dFGS redshift data.

The observations for this survey were carried out using the 6dF fibre-fed multi-object spectrograph at the United Kingdom Schmidt Telescope (UKST) over 2001 May to 2006 January (Jones et al. 2004). Target fields covered the $\sim$17 000 deg^2 of southern sky more than 10° from the Galactic plane,[4] approximately 10 times the area of the 2dFGRS (Colless et al. 2001) and more than twice the spectroscopic areal coverage of the SDSS Data Release 7 (DR7; Abazajian et al. 2009). Table 1 shows a comparison of the 6dFGS to these two major surveys. In terms of secure redshifts, 6dFGS has around half the number of 2dFGRS and one-sixth those of SDSS DR7 ($r < 17.77$). The comoving volume covered of 6dFGS is about the same as 2dFGRS at their respective median redshifts, and around

[1] 6dFGS home: http://www.aao.gov.au/6dFGS

[2] The 6dFGS magnitude limits in this final redshift release differ slightly from those reported in Jones et al. (2004, 2005) due to subsequent revision of the input magnitudes by Two Micron All-Sky Survey (2MASS) and SuperCOSMOS; see Section 2.

[3] http://www.aao.gov.au/6dFGS/Publications

[4] The $b_{\rm J}$ and $r_{\rm F}$ surveys of 6dFGS are limited to $|b| > 20°$ in order to mitigate the effect of higher Galactic extinction in the optical at lower latitudes.

Table 1. Comparison of recent wide-area low-redshift galaxy surveys.

	6dFGS	2dFGRS	SDSS-DR7
Magnitude limits	$K \leq 12.65$ $H \leq 12.95$ $J \leq 13.75$ $r_F \leq 15.60$ $b_J \leq 16.75$	$b_J \leq 19.45$	$r \leq 17.77$ (Petrosian)
Sky coverage (sr)	5.2	0.5	2.86
Fraction of sky	41 per cent	4 per cent	23 per cent
Extragalactic sample, N	125 071	221 414	644 951
Median redshift, $\tilde{z}$	0.053	0.11	0.1
Volume V in $[0.5\tilde{z}, 1.5\tilde{z}]$ $(h^{-3}\,\mathrm{Mpc}^3)$	2.1×10^7	1.7×10^7	7.6×10^7
Sampling density at $\tilde{z}$, $\bar{\rho} = (2N/3V)(h^3\,\mathrm{Mpc}^{-3})$	4×10^{-3}	9×10^{-3}	6×10^{-3}
Fibre aperture (arcsec)	6.7	2.0	3.0
Fibre aperture at $\tilde{z}$ $(h^{-1}\,\mathrm{kpc})$	4.8	2.8	3.9
Reference(s)	(1)	(2)	(3)

Note. Taking $h = H_0/100\,\mathrm{km\,s^{-1}\,Mpc^{-1}}$, $\Omega_{M_0} = 0.3$ and $\Omega_{\Lambda_0} = 0.7$. References: (1) this paper; (2) Colless et al. (2001), Cole et al. (2005); (3) Abazajian et al. (2009), www.sdss.org/dr7 (`PetroMag_r` < 17.77, `type` = 3, `zStatus` > 2 and objects with stellar morphology and $z > 0.001$).

30 per cent that of SDSS DR7. In terms of light-collection area, the larger apertures of 6dF (6.7 arcsec) give a projected diameter of $4.8\,h^{-1}$ kpc at the median redshift of the survey, covering 40 per cent more projected area than SDSS at its median redshift, and more than three times the area of 2dFGRS. By any measure, the scale of 6dFGS is readily comparable to those of SDSS and 2dFGRS, and like those surveys, its legacy is a permanent public data base, which is unique in its scope, depth and southern aspect.

Fig. 1 shows the sky distribution of 6dFGS targets and fields. Of the 1526 fields observed, 1447 contributed data to the final survey. The remaining 5 per cent were rejected for reasons of quality control, such as uniformly low signal-to-noise ratio data, of data that were unusable or corrupted in some way. In these cases the entire field was rejected. Of the 1447, around half have completeness greater than 90 per cent, and more than two thirds have completeness greater than 85 per cent. Although most sky regions are effectively covered twice, around 50 fields near the Large Magellanic Cloud (LMC) and the South Pole were not observed by the conclusion of the survey. Sky redshift completeness (Fig. 1c) is generally high (85 per cent or greater) but diminishes in regions with insufficient coverage or affected by poor conditions. In terms of survey limiting magnitude, $m_{\rm lim}$, completeness is greater than 85 per cent for $m < (m_{\rm lim} - 0.75)$ in fields with completeness 90 per cent or higher, and for $m < (m_{\rm lim} - 2)$ in fields with completeness 70 to 80 per cent.

2.2 Redshift distribution

The median redshift for 6dFGS is $\tilde{z} = 0.053$, roughly half that of SDSS and 2dFGRS, and twice that of the 2MASS Redshift Survey (2MRS; Erdogdu et al. 2006b). Fig. 2 shows the number distribution of 6dFGS redshifts for both the full sample, $N(z)$ (panel b; 125 071 sources), as well as the K-selected primary targets, $N_K(z)$ (panel c; 93 361). Both samples show the skewed distributions typical for magnitude-limited surveys, which is accentuated in Fig. 2(b) by the inclusion of additional target samples (Table 3, all ID > 10) that stretch the overall distribution to higher redshifts . This is also reflected in their interquartile ranges: [0.034, 0.074] for the full sample, compared to the slightly narrower [0.034, 0.070] for the K-selected sample. The localized peaks in $N(z)$ and $N_K(z)$ are due to individual large-scale structures, clearly seen in Fig. 2(a) when redshifts are spread across right ascension (RA). The gaps in (a) centred on RA 8 and 17 h correspond to the unsurveyed regions around the Galactic plane.

The limit of the K-selected sample ($K \leq 12.65$) encompasses galaxies with luminosities $M_K \leq -23.24$ at the median redshift ($\tilde{z} = 0.053$), around 0.6 mag fainter than M^*, the characteristic turnover point in the K-band luminosity function from the same sample (Jones et al. 2006). Integrating this luminosity function over the volume covered by 6dFGS in each redshift shell Δz yields the expected number–redshift distribution $N_{\rm LF}(z)$. As the K-band luminosity function contains completeness corrections that the raw $N_K(z)$ distribution does not, the ratio

$$\frac{\int_0^\infty N_K(z)\,\mathrm{d}z}{\int_0^\infty N_{\rm LF}(z)\,\mathrm{d}z} = 0.9245 \qquad (1)$$

is slightly less than unity. The blue dashed curve representing $N_{\rm LF}(z)$ in Fig. 2(c) has been scaled by this amount, and the ratio of the two distributions $N_K(z)/N_{\rm LF}(z)$ gives the normalization due to overall incompleteness. Any redshift differences between the curve and the data are due to magnitude-dependent incompleteness, which in turn imparts redshift differences in selection. Furthermore, a Schechter function is not a perfect fit to the luminosity function across all luminosities. The reader is referred to the 6dFGS luminosity function papers (Jones et al. 2006) for a more detailed discussion of survey selection functions.

The curve $N_{\rm LF}(z)$ (uncorrected for incompleteness) is well fit by the empirical function

$$N_{\rm fit}(z) = A\,z^\gamma\,\exp\left[-(z/z_{\rm p})^\gamma\right], \qquad (2)$$

with values $\gamma = 1.6154 \pm 0.0001$, $z_{\rm p} = 0.0446 \pm 0.0001$ and $A = 622980 \pm 10$ (Fig. 2c; red solid line, also scaled by 0.9245). This three-parameter function is a simpler variant of the four-parameter fits used by Erdogdu et al. (2006b) and Colless et al. (2001) for the 2MRS and 2dFGRS samples, respectively, but fits the 6dFGS K-band sample well. In this case, the value of $z_{\rm p}$ locates the peak in the distribution, which is slightly lower than the median of the data, and corresponds to a limiting absolute magnitude of $M_K = -22.97$ ($\sim$1 mag fainter than M^*). Even so, the remarkable consistency between the K-band luminosity function distribution $[N_{\rm LF}(z)]$ and that of the data $[N_K(z)]$ underscores the homogeneity of the primary sample.

2.3 Sample composition

The original target catalogue for 6dFGS contained 179 262 sources, one third of which originated from outside the NIR selected catalogues. Around 8 per cent of all targets had existing redshifts from ZCAT (9042; Huchra et al. 1992), the 2dFGRS (5210; Colless et al. 2001) or the SDSS DR7 (563; Abazajian et al. 2009). 6dFGS spectra were obtained in 136 304 source observations and yielded 126 754 unique redshifts of varying quality.

6dFGS redshift quality, Q, was classified on a scale of 1 to 6 through visual assessment of every redshift, with $Q = 1$ assigned to unusable measurements, $Q = 2$ to possible but unlikely redshifts, $Q = 3$ for reliable redshifts and $Q = 4$ for high-quality redshifts. Stars and other confirmed Galactic sources are assigned $Q = 6$ (there is no $Q = 5$). Some legitimate quasi-stellar object (QSO) redshifts classified earlier in the survey may carry $Q = 2$ from a time when no QSO-specific templates were employed, although in

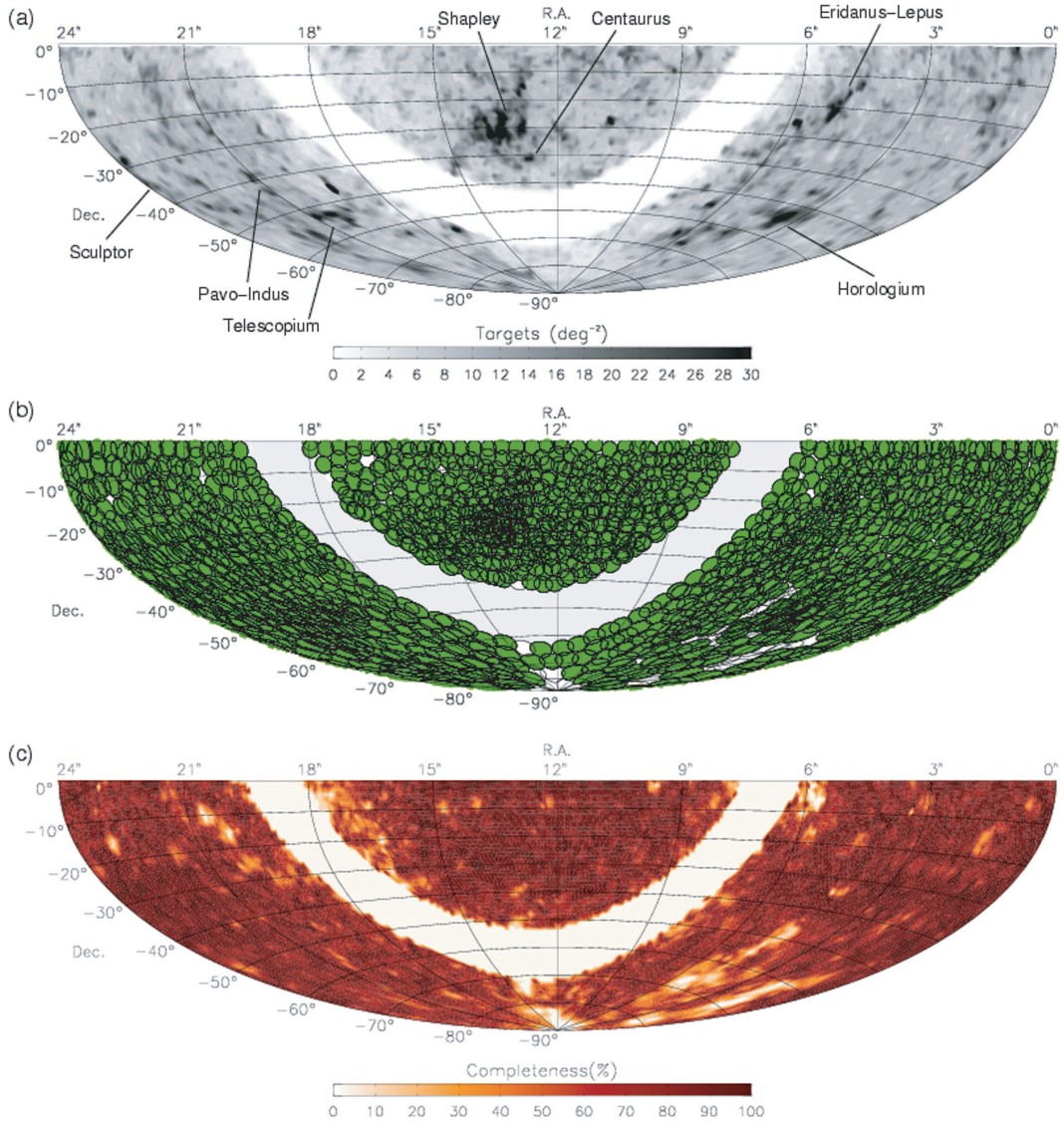

Figure 1. (a) Density of 6dFGS target sources (per square degree) on the sky; key supercluster overdensities are labelled. (b) Full 6dFGS field coverage (filled discs) and unobserved target fields (open circles). (c) Redshift completeness for $K \leq 12.65$. All panels show equal-area Aitoff projections.

most instances these classifications have been revised to $Q = 3$ or 4 (see Section 3.2). Unlike SDSS, no lower velocity limit has been used to discriminate between Galactic and extragalactic sources; assignment of $Q = 6$ is on the basis of spectral appearance as well as recession velocity. Cases of overlap between galaxies and foreground stars evident from imaging data were re-examined, and are discussed in Section 3. Table 2 gives the breakdown of these numbers across individual 6dFGS subsamples.

Only $Q = 3, 4$ redshifts should be used in any galaxy analysis. (The distinction between $Q = 3$ and $Q = 4$ is less important than that between $Q = 2$ and $Q = 3$, since the former represent a successful redshift in either case.) Galaxies with repeat observations have all spectra retained in the data base, and the final catalogued redshift is a weighted mean of the measurements with $Q = 3, 4$, excluding redshift blunders. Descriptions of the redshift quality scheme in its previous forms can be found in section 2.1 of Jones et al. (2005) and section 4.4 of Jones et al. (2004).

Unreliable ($Q = 2$) or unusable ($Q = 1$) galaxy redshifts together comprise around 8 per cent of the redshift sample. Galactic sources ($Q = 6$) represent another 4 per cent. The remaining 110 256 sources with $Q = 3, 4$ are the robust extragalactic 6dFGS redshifts that should be used (alongside the 14 815 literature redshifts) in any analysis or other application. Tables 2 and 3 give the breakdown of these numbers across various 6dFGS subsamples.

2.4 Redshift uncertainties and blunder rates

Redshift uncertainties and blunder rates were estimated from the sample of 6dFGS galaxies with repeat redshift measurements. We define a blunder as a redshift mismatch of more than 330 km s^{-1} (5σ) between a pair of redshift measurements that we would expect to agree. The blunder rate on individual 6dFGS redshifts is 1.6 per cent, the same as reported for the DR1 (Jones et al. 2004). In late 2002, new transmissive volume-phase holographic (VPH) gratings replaced the existing reflection gratings resulting in improved throughput, uniformity and data quality. Excluding first-year repeats reduces the individual blunder rate to 1.2 per cent. Table 4

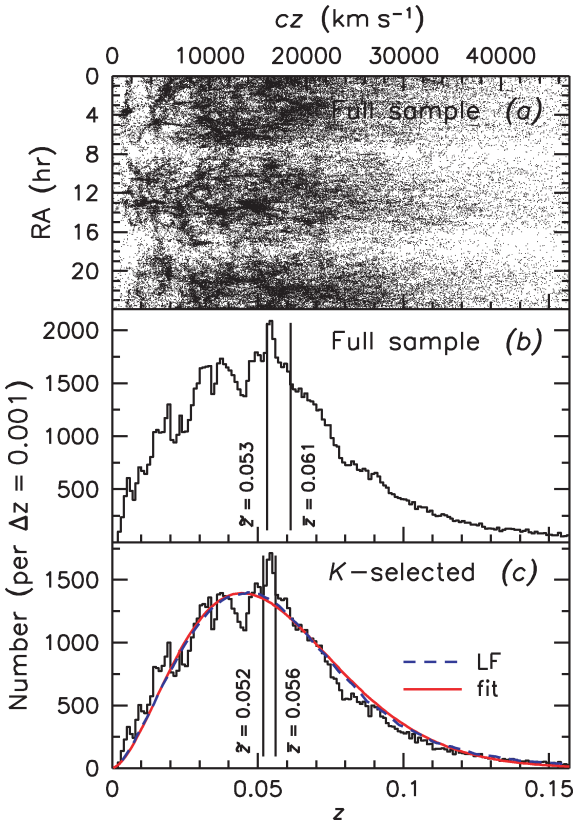

Figure 2. Distribution of all 6dFGS redshifts in terms of (a) RA and (b) number. Panel (c) shows the same as (b) but limited to the primary K-selected sample. The dashed blue line is the redshift distribution calculated from the K-band luminosity function of the same sample. The solid red line is an empirical fit to the blue curve. $\tilde{z}$ and $\bar{z}$ denote median and mean redshifts, respectively.

Table 2. Breakdown of 6dFGS and literature redshifts.

6dFGS by Q value	
$Q = 1$, unusable data	5 787 (4.6 pc)
$Q = 2$, unlikely redshifts	5 592 (4.4 pc)
$Q = 3$, reliable redshifts	8 173 (6.4 pc)
$Q = 4$, high-quality redshifts	102 083 (80.5 pc)
$Q = 6$, Galactic sources	5 119 (4.0 pc)
Total	126 754 (100 pc)
Literature redshifts	
SDSS	563 (3.8 pc)
2dFGRS	5 210 (35.2 pc)
ZCAT	9 042 (61.0 pc)
Total	14 815 (100 pc)

References. SDSS: Abazajian et al. (2009); 2dFGRS: Colless et al. (2001); ZCAT: Huchra et al. (1992).

summarizes the blunder rates and other statistics for both the full and post-first-year data.

Fig. 3 shows repeat redshift measurements for 6dFGS observations with the VPH gratings, representative of the great majority of survey spectra (around 80 per cent). There are 3611 $Q = 4$ non-blunder pairs with a scatter implying a $Q = 4$ redshift uncertainty of $\Delta cz(4) = 46\,\mathrm{km\,s^{-1}}$. Likewise, the scatter in the much smaller $Q = 3$ sample (33 pairs) suggests $\Delta cz(3) = 55\,\mathrm{km\,s^{-1}}$. There was minimal change in $\Delta cz(4)$ and $\Delta cz(3)$ after the gratings were changed, although blunder rates were much reduced (Table 4).

An external comparison of the 2459 6dFGS redshifts overlapping the DR7 of the SDSS (Abazajian et al. 2009) was also made and is shown in Fig. 4. The pair-wise blunder fraction is 3.9 per cent, implying an SDSS blunder rate of 2.7 per cent. However, we caution that the 6dFGS blunder rate at the fainter SDSS magnitudes is likely to be somewhat higher than the 1.2 per cent measured overall.

3 NEW DATA RELEASE

3.1 Online data base

The 6dFGS online data base is hosted at the Wide Field Astronomy Unit of the Institute for Astronomy[5] at the University of Edinburgh. Data are grouped into 15 interlinked tables consisting of the master target list, all input catalogues and their photometry. Users can obtain FITS and JPEG files of 6dFGS spectra as well as 2MASS and SuperCOSMOS postage stamp images in JHK and $b_J r_F$ where available, and a plethora of tabulated values for observational quantities and derived photometric and spectroscopic properties. The data base can be queried in either its native Structured Query Language (SQL) or via an HTML web-form interface. More complete descriptions are given elsewhere (Jones et al. 2004, 2005), although several new aspects of the data base are discussed below. Fig. 5 shows two examples of the way data are presented in the data base.

Table 5 shows the full parameter listing for the 6dFGS data base. Individual data base parameters are grouped into lists of related data called *tables*. Parameter definitions are given in documentation on the data base web site. The `TARGET` table contains the original target list for 6dFGS, and so contains both observed and unobserved objects. Individual entries in this table are celestial sources, and the `TARGETID` parameters are their unique integer identifiers. Note that the original target list *cannot* be used to estimate completeness, due to magnitude revisions in both the 2MASS XSC and SuperCOSMOS magnitudes subsequent to its compilation. Item (iv) below discusses this important issue in more detail.

The `SPECTRA` table holds the redshift and other spectroscopic data obtained by the 6dF instrument through the course of the 6dFGS. Many new parameters have been introduced to this table for this release (indicated in Table 5 by the superscript [a]). Individual entries in this table are spectroscopic observations, meaning that there can be multiple entries for a given object. The `SPECID` parameter is the unique integer identifier for 6dFGS observations.

Most 6dFGS spectra consist of two halves, observed separately through different gratings, and subsequently spliced together: a V portion ($\lambda\lambda$3900–5600 Å) and an R portion ($\lambda\lambda$5400–7500 Å).[6] (Data taken prior to 2002 October used different gratings, spanning 4000–5600 and 5500–8400 Å.) Various parameters in `SPECTRA` belonging to the individual V or R observations carry a `_V` or `_R` suffix, and are listed in Table 5 for V (with slanted font to indicated that there is a matching set of R parameters).

The `TWOMASS` and `SUPERCOS` tables hold relevant 2MASS XSC and SuperCOSMOS photometric and spatial information. Likewise, the remaining 11 tables contain related observables from the input lists contributing additional 6dFGS targets to `TARGET`. While some of the parameter names have been duplicated between tables (e.g. `MAG_1`, `MAG_2`) their meaning changes from one table to the next, as indicated in Table 5.

[5] http://www-wfau.roe.ac.uk/6dFGS

[6] V and R here are not related to standard V or R passbands.

Table 3. Final numbers of spectra and redshifts in the 6dFGS samples.

ID	Survey sample	6dFGS spectra	Good z	Lit. z	Total z
1	2MASS $K_s \leq 12.65$	97 020	83 995	9 340	93 335
3	2MASS $H \leq 12.95$	2 021	1 742	255	1 997
4	2MASS $J \leq 13.75$	1 284	1 096	175	1 271
5	DENIS $J \leq 14.00$	629	488	115	603
6	DENIS $I \leq 14.85$	504	234	109	343
7	SUPERCOS $r_F < 15.60$	5 773	5 025	1 221	6 246
8	SUPERCOS $b_J < 16.75$	6 516	5 885	1 236	7 121
78	Dur./UKST extension	271	207	30	237
90	Shapley supercluster	630	494	40	534
109	Horologium sample	469	384	41	425
113	*ROSAT* All-Sky Survey	1 961	1 126	190	1 316
116	2MASS red AGN	1 141	438	140	578
119	HIPASS ($>4\sigma$)	439	354	116	470
125	SUMSS/NVSS radio	2 978	1 351	272	1 623
126	*IRAS* FSC ($>6\sigma$)	5 994	4 208	1 239	5 447
129	Hamburg-ESO QSOs	2 006	624	123	747
130	NRAO-VLA QSOs	2 673	293	41	334
≥ 999	Unassigned targets[a]	3 995	2312	132	2 444
	Total	136 304	110 256	14 815	125 071

Note. Columns:
(1) ID: programme ID (PROGID in the data base; see Section 3).
(2) Survey sample: first sample (in order of PROGID) in which object is found.
(3) 6dFGS spectra: number of spectra obtained for this sample. Note that some objects were observed more than once. The numbers include spectra of all qualities and Galactic sources.
(4) Good z: number of robust extragalactic 6dFGS redshifts, (those with $Q = 3$ or 4). Reflects contents of data base.
(5) Lit. z: additional literature extragalactic redshifts (ignoring repeats and overlaps).
(6) Total z: total number of extragalactic redshifts for objects in this sample.
[a]Objects removed from the initial target list (due to changes in the 2MASS source catalogue after 6dFGS was underway). ID = 999 or 9999 in these cases.

Table 4. Redshift uncertainties and blunder rates from both internal and external comparisons of 6dFGS.

6dFGS (full sample)	
Total repeat measurements ($Q \geq 3$)	8028
rms scatter of all redshift measurement pairs[a]	66 km s^{-1}
$Q = 4$ redshift uncertainty (6051 sources)	45 km s^{-1}
$Q = 3$ redshift uncertainty (104 sources)	67 km s^{-1}
Number of blunders[b] ($Q \geq 3$)	260
6dFGS pair-wise blunder rate	3.2 per cent
6dFGS single-measurement blunder rate	1.6 per cent
6dFGS (VPH grating only, 2002.5–2006)	
Total repeat measurements ($Q \geq 3$)	4570
rms scatter of all redshift measurement pairs[a]	67 km s^{-1}
$Q = 4$ redshift uncertainty (3611 sources)	46 km s^{-1}
$Q = 3$ redshift uncertainty (33 sources)	55 km s^{-1}
Number of blunders[b] ($Q \geq 3$)	106
6dFGS pair-wise blunder rate	2.3 per cent
6dFGS single-measurement blunder rate	1.2 per cent
6dFGS (VPH only) versus SDSS DR7	
Number of comparison sources ($Q \geq 3$)	2459
Number of blunders[a] ($Q \geq 3$)	95
Pair-wise blunder rate	3.9 per cent
Implied blunder rate for SDSS	2.7 per cent

[a]Clipping the most extreme 10 per cent of outliers (5 per cent either side).
[b]A blunder is defined as having $\Delta cz > 330$ km s^{-1} (5σ).

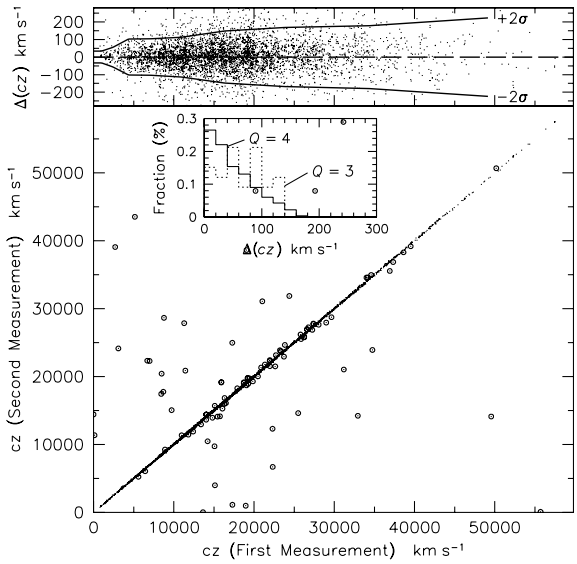

Figure 3. Bottom panel: repeat 6dF redshift measurements for a sample of 6dFGS galaxies obtained with the VPH gratings over the period 2002.5 to 2006 (4570 galaxies). Redshift blunders (circled) are those for which $|\Delta cz| > 330$ km s^{-1}. Inset: distribution of the $|\Delta cz|$ differences for the individual redshift quality $Q = 3$ (dotted line) and $Q = 4$ (solid line) samples, normalized to the total sample size in each case. Top panel: distribution of redshift difference as a function of redshift, with a running $\pm 2\sigma$ boundary (solid lines).

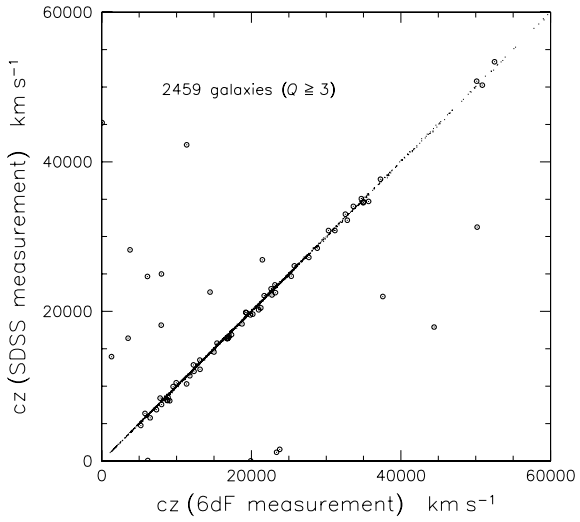

Figure 4. Redshift comparison of 6dFGS (VPH grating) with SDSS DR7 (Abazajian et al. 2009).

Data base tables can be queried individually or in pairs. Alternatively, positional cross-matching [RA and declination (Dec.)] can be done between data base sources and those in a user-supplied list uploaded to the site. Search results can be returned as HTML-formatted tables, with each entry linking to individual GIF frames showing the 6dFGS spectrum alongside its $b_J r_F$ JHK postage stamp images, as shown in Fig. 5. Individual object FITS files of the same data can also be accessed in this way. Long data base returns can also be e-mailed to the user as an ASCII comma-separated variable (CSV) text file. Alternatively, the FITS files of all objects found through a search can be e-mailed to the user as a single tar file under a *TAR saveset* option.

Additional downloads in the form of ASCII files are also available from the data base web site. These include a master catalogue compilation of all redshifts (from both 6dFGS and the literature), as well as a comma-separated file of the spectral observations. The latter contains an entry for every 6dFGS observation held by the data base (including repeats), regardless of redshift quality. The master catalogue attempts to assign the best available redshift to those sources determined to be extragalactic. In the case of repeats, a combined 6dFGS redshift is obtained by error weighting $[1/(\Delta cz)^2]$ those $Q = 3, 4$ redshifts within 5σ ($330\,\mathrm{km\,s^{-1}}$) of an initial $Q = 3, 4$ median, thereby excluding blunders. Where literature redshifts exist and are consistent with the 6dFGS redshift, the latter is used in the catalogue. In cases of disagreement ($>5\sigma$ difference), the 6dFGS redshift is taken and the mismatch is flagged. Literature redshifts are used, where they exist, for objects that 6dFGS failed to secure. The master catalogue includes the `TARGETID` for each object and the `SPECID` references for each 6dFGS observation contributing to the final redshift, to facilitate cross-referencing with the 6dFGS data base. Completeness maps (calculated from the revised target lists, after 2MASS and SuperCOS magnitude changes) will be made available through the 6dFGS web site when completed.

Table 6 lists a subset of the more commonly used data base parameters, along with detailed descriptions. New parameters for this final release are indicated. Users should pay particular attention to the important differences between parameters which have similar-sounding names but which are significantly different in purpose. Examples to note are (i) `Z`, `Z_ORIGIN`, `Z_HELIO`, `Z_INITIAL` and `Z_HELIO_INITIAL`, (ii) `QUALITY` and `Q_FINAL`, (iii) (`JTOT`, `HTOT`, `KTOT`), (`J`, `H`, `K`) and (`MAG1`, `MAG2`) (from the `TWOMASS` table) and (iv) (`BMAG`, `RMAG`), (`BMAGSEL`, `RMAGSEL`) and (`BMAG`, `RMAG`) (from the `SUPERCOS` table). Table 6 details the differences between them.

3.2 Changes made for the final redshift release

All of the changes previously implemented for DR2 (Jones et al. 2005) have been retained, with some modifications. In particular, some fields rejected from earlier data releases on technical grounds have been fixed and included in the final release. The final data span observations from 2001 May to 2006 January inclusive. New changes are as follows.

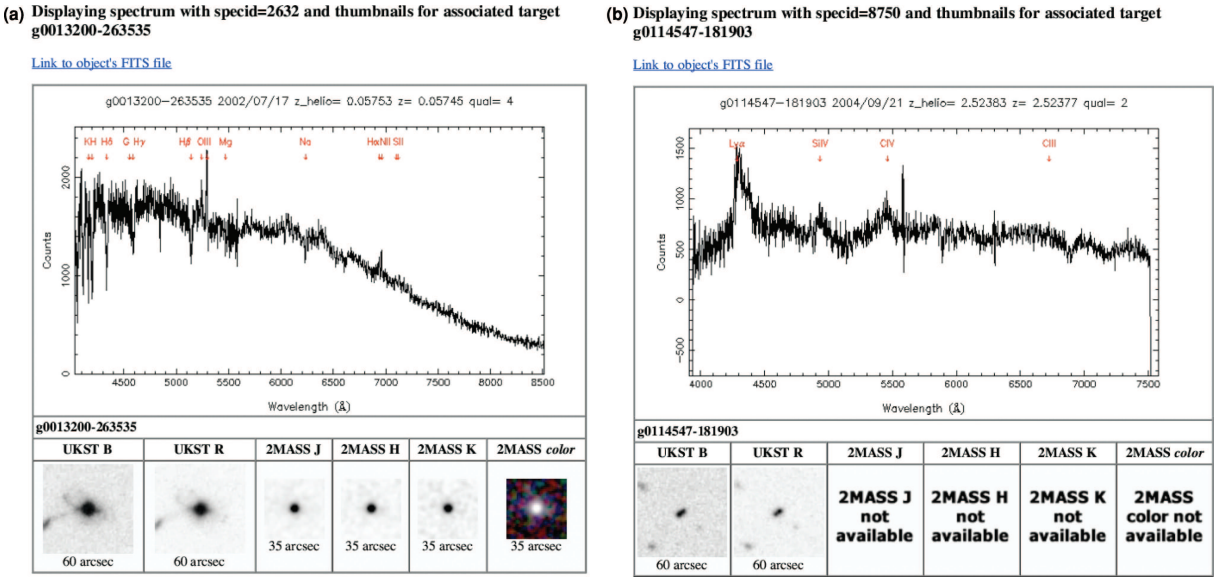

Figure 5. Example spectroscopic and photometric frames from the 6dFGS online data base for (a) a nearby bright galaxy at $z = 0.057$ ($Q = 4$) from the K-selected sample (`PROGID` = 1), and (b) a candidate double QSO at $z = 2.524$ ($Q = 2$) from the Hamburg-ESO QSO sample (`PROGID` = 129). 2MASS and UKST frames are only available for sources selected as part of the original 6dFGS primary samples, where available in one or more of $KHJr_F b_J$.

Table 5. Full parameter listing for all tables in the 6dFGS data base.

Table name	Description	PROGID	Parameters
TARGET	The master target list	–	TARGETID, TARGETNAME, HTMID, RA, DEC, CX, CY, CZ, GL, GB, A_V, PROGID, BMAG, RMAG, SG, ZCATVEL, ZCATERR, ZCATREF, BMAGSEL, RMAGSEL, TEMPLATECODE[a], FRAMENAME
SPECTRA	Redshifts and observational data	–	SPECID, TARGETID, TARGETNAME, OBSRA, OBSDEC, MATCH_DR, HTMID, CX, CY, CZ, Z_ORIGIN, Z, Z_HELIO, QUALITY, ABEMMA, NMBEST, NGOOD, Z_EMI, Q_Z_EMI, KBESTR, R_CRCOR, Z_ABS, Q_Z_ABS, Q_FINAL, IALTER, Z_COMM, ZEMIBESTERR, ZABSBESTERR, ZFINALERR, *TITLE_V, CENRA_V, GRATSLOT_V, CENDEC_V, APPRA_V, APPDEC_V, ACTMJD_V, CONMJD_V, PROGID_V, LABEL_V, OBSID_V, RUN_V, EXP_V, NCOMB_V, GRATID_V, GRATSET_V, GRATBLAZ_V, SOURCE_V, FOCUS_V, TFOCUS_V, GAIN_V, NOISE_V, CCD_V, UTDATE_V, UTSTRT_V, MJDOBS_V, NAME_V, THPUT_V, RA_V, DEC_V, X_V, Y_V, XERR_V, YERR_V, THETA_V, FIBRE_V, PIVOT_V, RECMAG_V, PID_V,* FRAMENAME, *AXISSTART_V, AXISEND_V,* MATCHSPECID, Z_INITIAL[a], Z_HELIO_INITIAL[a], Z_UPDATE_FLAG[a], Z_UPDATE_COMM[a], SLIT_VANE_CORR[a], QUALITY_INITIAL, XTALKFLAG[a], XTALKSCORE[a], XTALKVELOFF[a], XTALKCOMM[a], QUALITY_UPDATE_COMM, DEPRECATED[a] REVTEMPLATE[a], REVCOMMENT[a], Z_COMM_INITAL[a]
TWOMASS	*JHK* 2MASS input catalogues	1 (*K*), 3 (*H*), 4 (*J*)	OBJID, CATNAME, TARGETNAME, TARGETID, RA, DEC, PRIORITY, MAG_1, PROGID, MAG_2, J_M_K20FE, H_M_K20FE, K_M_K20FE, RADIUS, A_B, MUK20FE, CORR, J, H, KEXT, K, KEXT_K, PREVCATNAME[a], RTOT[a], JTOT[a], HTOT[a], KTOT[a]
SUPERCOS	b_J r_F SuperCOSMOS input catalogues	8 (b_J), 7 (r_F)	OBJID, CATNAME, TARGETNAME, TARGETID, RA, DEC, PRIORITY, MAG_1 (old b_J), PROGID, MAG_2 (old r_F), COMMENT
FSC	*IRAS* Faint Source Catalogue sources	126	OBJID, CATNAME, TARGETNAME, TARGETID, RA, DEC, PRIORITY, MAG_1, PROGID, MAG_2, COMMENT
RASS	*ROSAT* All-Sky Survey candidate AGN	113	OBJID, CATNAME, TARGETNAME, TARGETID, RA, DEC, PRIORITY, MAG_1, PROGID, MAG_2, COMMENT
HIPASS	Sources from the HIPASS HI survey	119	OBJID, CATNAME, TARGETNAME, TARGETID, RA, DEC, PRIORITY, MAG_1, PROGID, MAG_2
DURUKST	Durham/UKST galaxy survey extension	78	OBJID, CATNAME, TARGETNAME, TARGETID, RA, DEC, PRIORITY, MAG_1, PROGID, MAG_2
SHAPLEY	Shapley supercluster galaxies	90	OBJID, CATNAME, TARGETNAME, TARGETID, RA, DEC, PRIORITY, MAG_1, PROGID, MAG_2
DENISI	DENIS survey galaxies, $I < 14.85$	6	OBJID, CATNAME, TARGETNAME, TARGETID, RA, DEC, PRIORITY, MAG_1, PROGID, MAG_2, COMMENT
DENISJ	DENIS survey galaxies, $J < 13.85$	5	OBJID, CATNAME, TARGETNAME, TARGETID, RA, DEC, PRIORITY, MAG_1, PROGID, MAG_2, COMMENT
AGN2MASS	2MASS red AGN survey candidates	116	OBJID, CATNAME, TARGETNAME, TARGETID, RA, DEC, PRIORITY, MAG_1, PROGID, MAG_2, MAG_3
HES	Hamburg/ESO survey candidate QSOs	129	OBJID, CATNAME, TARGETNAME, TARGETID, RA, DEC, PRIORITY, MAG_1, PROGID, MAG_2
NVSS	Candidate QSOs from NVSS	130	OBJID, CATNAME, TARGETNAME, TARGETID, RA, DEC, PRIORITY, MAG_1, PROGID, MAG_2
SUMSS	Bright radio sources from SUMSS	125	OBJID, CATNAME, TARGETNAME, TARGETID, RA, DEC, PRIORITY, MAG_1, PROGID, MAG_2

Note. *Slanted font* V-spectrum parameters (*_V*) have matching R-spectrum (*_R*) parameters.
[a]New parameters created for the final data release.

(i) *Revised 2MASS names.* 2MASS changed their source designations (in the last two digits of RA and Dec.) between 2001 and 2004. The original 2MASS names have been retained but rebadged under a new attribute PREVCATNAME. The revised 2MASS names are stored in CATNAME and are consistent with the final data release of the 2MASS XSC. Original 6dFGS sources that were subsequently omitted from the final 2MASS data release have CATNAME = ' '.

(ii) *Revised 2MASS photometry.* The *JHK* total magnitudes used to select 6dFGS sources were also revised by 2MASS, and are held in the newly created JTOT, HTOT and KTOT parameters. The revisions amount to less than 0.03 mag, except in the case of corrected blunders. The old magnitudes used for target selection continue to be held in J, H and KEXT_K.

(iii) *Revised SuperCOSMOS photometry.* Improvements to the algorithm we have used to match 6dFGS objects with new SuperCOSMOS magnitudes have seen some BMAG and RMAG change. This has removed much more of the deblending discussed in section 2.3 of Jones et al. (2005). The historical $b_J r_F$ magnitudes held in BMAGSEL, RMAGSEL (in the TARGET table) and MAG_1, MAG_2 (in the SUPERCOS table) retain their DR2 definitions and values. BMAG and RMAG are the $b_J r_F$ magnitudes that should be used for science purposes.

Table 6. Descriptions of some key parameters in the 6dFGS data base.

Parameter	Associated table(s)	Notes
TARGETID	All	Unique source ID (integer), used to link tables.
TARGETNAME	All	Source name, 'g#######.##−#######'. (Sources observed but not in the original target list have the form 'c#######−#######').
PROGID	All	Programme ID (integer), identifying the origin of targets. PROGID ≤ 8 for main samples.
OBJID	All except TARGET and SPECTRA	Unique object ID (integer), assigned to each object in all input catalogues.
BMAG,RMAG	TARGET	New $b_{\rm J}$ $r_{\rm F}$ SuperCOSMOS magnitudes following the revision for 2dFGRS by Peacock, Hambly and Read. First introduced for DR2. The most reliable $b_{\rm J}$ $r_{\rm F}$ 6dFGS magnitudes.
ZCATVEL,ZCATERR	TARGET	Existing redshifts and errors (km s^{-1}) from ZCAT (Huchra et al. 1992) where available.
ZCATREF	TARGET	Code indicating source of ZCAT redshift: '126x' for earlier 6dFGS redshifts (subsequently ingested by ZCAT), '392x' for ZCAT-ingested 2dFGRS redshifts. The 'x' in both cases holds redshift quality (see QUALITY below). ZCATREF ≤ 99 for other ZCAT surveys.
BMAGSEL,RMAGSEL	TARGET	Old $b_{\rm J}r_{\rm F}$ SuperCOSMOS magnitudes compiled by W. Saunders. Never used for selection and not intended for science. Previously under BMAG and RMAG in pre-DR2 releases.
TEMPLATECODE	TARGET	Code indicating cross-correlation template: 'N' = no redshift, 'Z' = ZCAT redshift (no template used), 'T' = 2dFGRS (no template used), 1 . . . 9 = 6dFGS template code.
SPECID	SPECTRA	Unique spectral ID (integer). Different for repeat observations of the same object.
Z_ORIGIN	SPECTRA	Is 'C' for most spectra, which come from (c)ombined (spliced) V and R spectral frames. Is 'V' or 'R' for unpaired (orphan) data, as applicable.
KBESTR	SPECTRA	Template spectrum ID (integer) used for redshift cross-correlation.
Z_HELIO	SPECTRA	Heliocentric redshift. Corrected by -40 km s^{-1} for template offset if KBESTR = 1 or 7. The redshift intended for science use.
Z	SPECTRA	Raw measured redshift. Not intended for science use. Also template offset corrected.
Z_INITIAL[a]	SPECTRA	Initial copy of redshift Z, uncorrected (e.g. for slit vane shifts). Not for scientific use.
Z_UPDATE_FLAG[a]	SPECTRA	Z_HELIO corrections: '1' if slit–vane corrected, '2' if template corrected, '3' for both.
Z_HELIO_INITIAL[a]	SPECTRA	Initial version of Z_HELIO, uncorrected (e.g. for slit vane shifts). Not for science use.
QUALITY	SPECTRA	Redshift quality, Q (integer): '1' for unusable measurements, '2' for possible but unlikely redshifts, '3' for a reliable redshift, '4' for high-quality redshifts, and '6' for confirmed Galactic sources. Only QUALITY = 3 or 4 should be used for science. (QUALITY does *not* measure spectral quality.)
Q_FINAL	SPECTRA	Final redshift quality assigned by software. Not intended for general use. Use QUALITY.
QUALITY_INITIAL[a]	SPECTRA	Quality value at initial ingest, before data base revision. Not for general use.
QUALITY_UPDATE_COMM[a]	SPECTRA	Explanation of quality value changes during data base revision.
TITLE_V,TITLE_R	SPECTRA	Observation title from SDS configuration file (consisting of field name and plate number).
XTALKFLAG[a]	SPECTRA	Fibre number of a nearby object suspected of spectral cross-talk contamination. '−1' if object is a contaminator itself. '0' if neither a contaminator nor contaminee.
XTALKSCORE[a]	SPECTRA	Score from '0' (none) to '5' (high) assessing the likelihood of spectral cross-contamination.
XTALKVELOFF[a]	SPECTRA	Velocity offset (km s^{-1}) between contaminator and contaminee in cross-contamination.
XTALKCOMM[a]	SPECTRA	Comment about cross-talk likelihood.
SLIT_VANE_CORR[a]	SPECTRA	Correction (km s^{-1}) made to a redshift affected by slit vane shifts during observing.
REVTEMPLATE[a]	SPECTRA	Code of any spectral template used during the data base revision of redshifts.
REVCOMMENT[a]	SPECTRA	Explanation of any redshift changes resulting from the data base revision.
CATNAME	TWOMASS	2MASS name. (Prior to this release, CATNAME held the old names now in PREVCATNAME).
PREVCATNAME[a]	TWOMASS	Old 2MASS name (as at 2001).
RTOT[a]	TWOMASS	2MASS XSC extrapolated/total radius (2MASS r_ext parameter).
JTOT,HTOT,KTOT[a]	TWOMASS	Revised 2MASS XSC total *JHK* magnitudes (2MASS j_m_ext, etc.). For science use.
MAG_1,MAG_2	TWOMASS	Input catalogue magnitudes. Not used in TWOMASS table and so default non-value is 99.99. Superseded by JTOT, HTOT and KTOT.
CORR	TWOMASS	Magnitude correction (based on average surface brightness) used to calculate KEXT_K.
J,H,K	TWOMASS	Old 2MASS XSC total *JHK* magnitudes. *JH* used for selection. Superseded by JTOT, etc.
KEXT	TWOMASS	Redundant 2MASS extrapolated K magnitudes, previously used to obtain KEXT_K.
KEXT_K	TWOMASS	Old total K magnitude estimated from KEXT and CORR. Used in original 6dFGS K-band selection (see Jones et al. 2004 for a discussion). Now redundant.
MAG_1,MAG_2	SUPERCOS	Old $b_{\rm J}$ $r_{\rm F}$ SuperCOSMOS magnitudes compiled by Saunders, Parker and Read for target selection. Now superseded by the revised magnitudes BMAG and RMAG in the TARGET table.

[a]New parameters created for the final data release.

(iv) *Redshift completeness.* The 2MASS and SuperCOSMOS magnitude revisions have imparted a $\lesssim 0.5$ mag scatter between the old and new versions of $b_{\rm J}r_{\rm F}$ JHK, particularly $b_{\rm J}r_{\rm F}K$. This has a non-negligible impact on estimates of 6dFGS redshift completeness at the faint end (faintest $\sim$0.5 mag) of each distribution, and previous users of the catalogue interested in completeness should make allowance for this.

(v) *Fibre cross-talk.* Instances of fibre cross-talk, in which bright spectral features from one spectrum overlap with an adjacent one, have been reviewed and are now flagged in the data

base through three new parameters: XTALKFLAG, XTALKSCORE and XTALKVELOFF. Users are urged to use extreme caution with redshifts from sources having XTALKFLAG ≥ 1, XTALKVELOFF > 0 and XTALKSCORE ≥ 4. Cases of XTALKSCORE $= 3$ are weak candidates where cross-talk is possible but not fully convincing. XTALKSCORE $= 4$ are good candidates, but which carry the previous caveat. XTALKSCORE $= 5$ are likely cross-talk pairs which are usually confirmed through visual inspection of the spectra. Cross-talk is an uncommon occurrence (about $\sim$1 per cent of all spectra), and it only affects the redshifts for spectra with fewer real features than false ones. A detailed discussion of the cross-talk phenomenon can be found in the data base documentation on the web site.

(vi) *Highest redshift sources.* Spurious features due to cross-talk or poor sky subtraction can create erroneously high redshifts, especially for the additional target samples (PROGID > 8), whose selection criteria are less well matched to the limiting magnitudes of 6dFGS spectra. Special care should be taken with the high-redshift sources reported for these targets. All sources (across all programmes) with $z \geq 1.0$ were re-examined and reclassified where necessary. In addition, those sources from the primary and secondary samples (PROGID ≤ 8) with redshifts in the range $0.2 \leq z < 1.0$ were re-examined. There are 318 6dFGS sources with $z > 1$, mostly QSOs, and a further seven possible cases. The highest of these is the $z = 3.793$ QSO g2037567−243832. Other notable examples are the candidate double QSO sources g0114547−181903 ($z = 2.524$) shown in Fig. 5(b) and g2052000−500523 ($z = 1.036$). Deep follow-up imaging in search of a foreground source is necessary to decide whether these sources are individual gravitationally lensed QSOs or genuine QSO pairs.

(vii) *Orphan fields.* The final data release includes (for the first time) data from 29 orphan fields. These are fields that, for various reasons, are missing either the V or R half of the spectrum. Orphan field data are flagged in the data base through the Z_ORIGIN parameter.

(viii) *Re-examination of $Q = 1$ and $Q = 2$ spectra.* All sources originally classified as either being extragalactic and $Q = 2$ or non-2MASS selected (PROGID > 4) and $Q = 1$ have been re-examined. This was done primarily to improve the identification of faint high-redshift QSOs.

(ix) *Image examination of all $Q = 6$ sources and reredshifting.* The 6212 sources originally classified as $Q = 6$ (i.e. confirmed Galactic sources with $z = 0$) had their redshifts re-examined alongside their postage-stamp images. Of these, 847 were found to be galaxies with near-zero redshifts, which were subsequently reredshifted and reclassified. In some cases, even though the source was clearly a galaxy in the image, its true redshift could not be obtained. The most common causes were scattered light from a nearby star, or contamination from a foreground screen of Galactic emission. Users interested in nearby galaxies ($cz < 1200\,\mathrm{km\,s^{-1}}$) should exercise special care in this regard.

(x) *Anomalous K–z sources with $Q = 3, 4$.* The K–z magnitude–redshift relation was used to identify anomalous redshifts ($Q = 3$, 4) outside the envelope normally spanned by this relation. There were 120 objects deemed to have an anomalous K–z; 94 were found to have incorrect redshifts, which were corrected.

(xi) *Correction of slit–vane shifted fields.* Mid-way through the survey it became apparent that the magnetically held vane supporting the spectrograph slit was shifting occasionally between exposures. This problem was discovered prior to DR2 but the affected redshifts were withheld; they have been corrected and provided in the final release. The resulting spectra from affected fields show a small wavelength offset (greater than ± 0.75 Å and up to a few Å), dependent on fibre number. The V and R spectral halves were sometimes affected individually, and at other times in unison. Instances of shifting were isolated by comparing the wavelength of the [O I]λ5577.4 Å sky line, as measured from the 6dFGS spectra, to its true value. A search found 125 affected fields able to be satisfactorily fit (measured [O I] against fibre number) and redshift corrected. In all, 18 438 galaxies were corrected in this way (approximately 14 per cent of the entire sample of *all* spectra), with corrections $\lesssim$12 Å. Redshift template values KBESTR were used to determine whether to apply a correction. If an object used KBESTR $= 1, 2$ (corresponding to early-type galaxy templates), the redshift was deemed to be due to absorption lines, which occur predominantly in the V half. If the corresponding V frame was indeed slit–vane affected, a correction was applied to the redshift for this galaxy based on the fit to the V frame *alone*. Alternatively, if KBESTR $=3, 4, 5$ (corresponding to late-type galaxy templates), then the redshift was deemed to be emission-line dependent, and the corresponding R frame correction was made where necessary. Users can find those galaxies with slit–vane corrected redshifts through the new SLITVANECORR parameter, which gives the size (in $\mathrm{km\,s^{-1}}$) of any corrections applied. Unaffected galaxies have SLITVANECORR $= 0$. The corrected redshifts are the heliocentric redshifts held by Z_HELIO.

(xii) *Correction for template offset values.* Various tests comparing 6dFGS redshifts to independent measurements found small systematic offsets in the case of a couple of templates. The discrepancy is almost certainly due to a zero-point error in the velocity calibration of the template spectra. This effect was discovered prior to DR2 and is discussed in Jones et al. (2005), although no corrections were applied to the affected redshifts in that release. For this final release, corrections of $-40\,\mathrm{km\,s^{-1}}$ have been applied to redshifts derived from templates KBESTR=1, 7. The corrected redshifts are both the raw (Z) and heliocentric (Z_HELIO) redshifts. The redshift offsets were found to be consistent between a 2004 comparison of 16 127 6dFGS and ZCAT redshifts, and a 2007 comparison of 443 redshifts from various peculiar velocity surveys (Smith et al. 2000, 2004; Bernardi et al. 2003; Wegner et al. 2003).

(xiii) *Telluric sky line subtraction.* The redshifting software used by 6dFGS automatically removed telluric absorption lines from spectra, but the data base spectra have hitherto retained their imprint. For the final release we have respliced spectra and incorporated telluric line removal. Those spectra that failed to resplice successfully have had their old telluric-affected versions retained.

(xiv) *Spurious clustering.* The entire sample of reliable redshifts ($Q = 3, 4$) was tested for spurious clusters, caused by any systematic effect that produces noticeable numbers of objects from the same field with nearly identical redshifts. Possible causes include poor sky subtraction and/or splicing of spectra, and the fibre cross-talk effect discussed in item (v). Fields containing at least 16 cases of galaxy groups (three or more members) with redshift differences of less than $30\,\mathrm{km\,s^{-1}}$ had their redshifts re-examined: 171 galaxies from seven fields. No prior knowledge of real galaxy clustering was used for the reredshifting. The field 0058m30 was particularly prominent with 48 galaxies at or near an apparent redshift of 0.1590 (due to the oversubtraction and subsequent misidentification of the 7600 Å telluric absorption band with redshifted Hα). Almost all of the affected spectra are among the earliest observations of survey data (2001), prior to the switch to VPH gratings.

(xv) *RASS sources.* All sources in the *ROSAT* All-Sky Survey (RASS) additional target sample (PROGID $= 113$; 1850 sources) were re-examined and updated using the full QSO template set. Mahoney et al. (2009) describe the selection and characteristics of this sample in more detail.

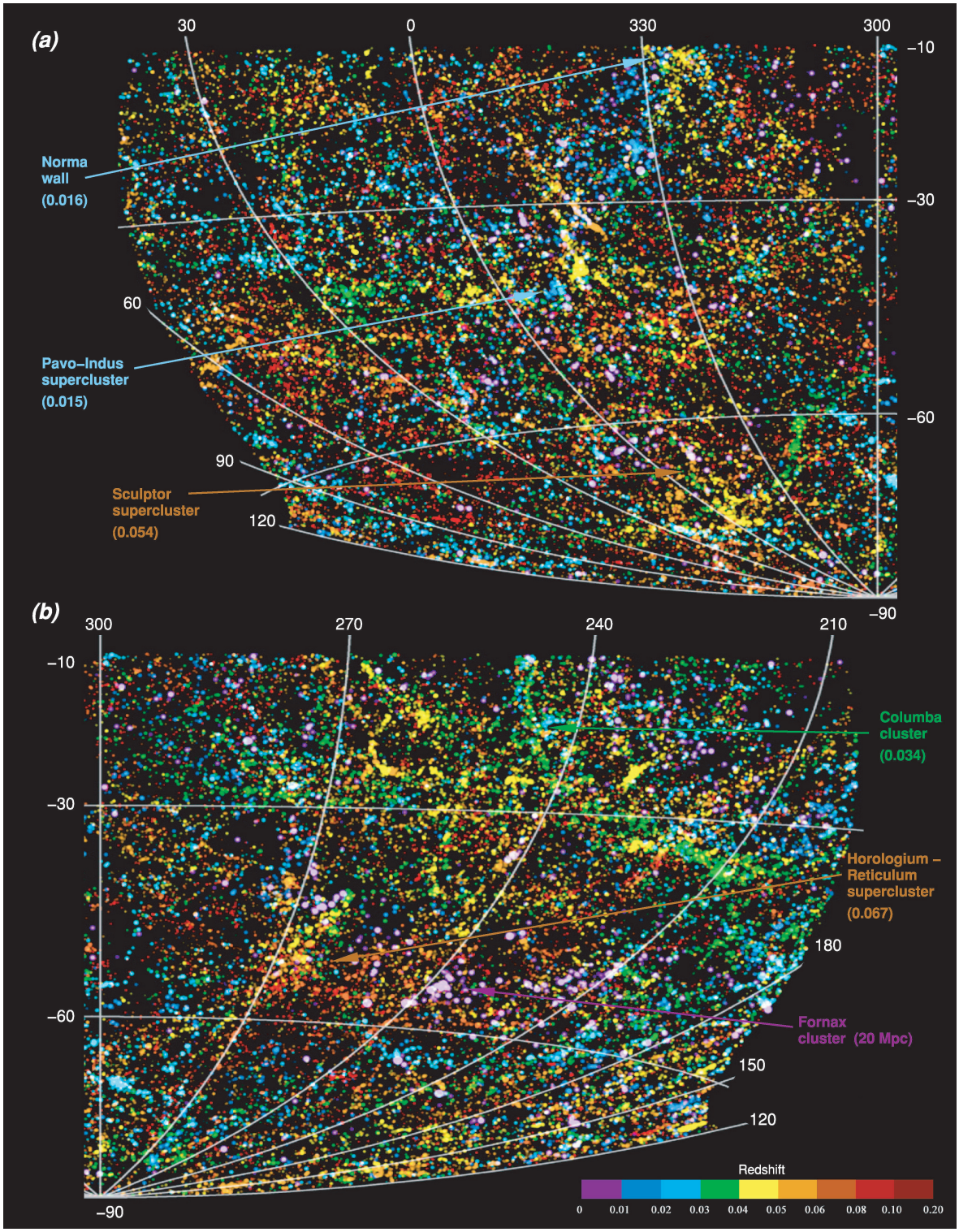

Figure 6. The distribution of galaxies in the 6dFGS shown in an Aitoff projection of Galactic coordinates across the Southern Galactic hemisphere; redshifts are colour coded from blue (low, $z < 0.02$) to red (high, $z > 0.1$). Some of the major large-scale structures are labelled.

4 SOUTHERN LARGE-SCALE STRUCTURES

4.1 Sky projections

The wide sky coverage of the 6dFGS affords the most detailed view yet of southern large-scale structures out to $cz \sim 30\,000\,\mathrm{km\,s^{-1}}$. The 6dFGS extends the sky coverage of the 2dFGRS (Colless et al. 2001) by an order of magnitude, and likewise improves by an order of magnitude on the sampling density of the all-sky Point Source Catalog redshift (PSCz) survey (Branchini et al. 1999; Saunders et al. 2000). Major strengths of the 6dFGS are that it affords contiguous coverage of the southern sky and extends much further

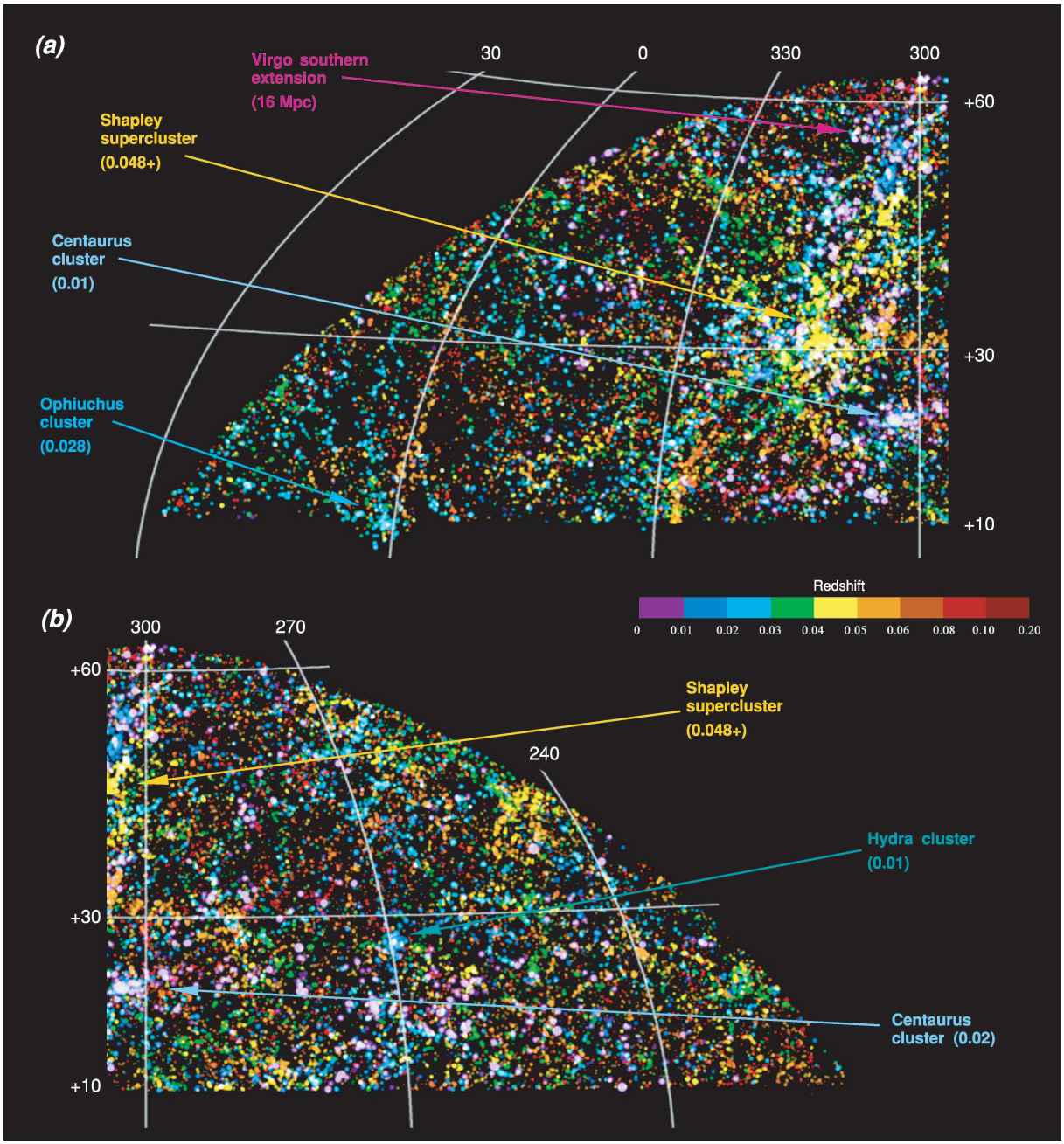

Figure 7. Same as Fig. 6 except showing the Northern Galactic hemisphere.

south than either 2dFGRS or SDSS. Prominent southern structures such as Shapley, Hydra-Centaurus and Horologium-Reticulum have received much special attention in their own right over recent years (Raychaudhury 1989; Quintana et al. 1995; Drinkwater et al. 1999; Bardelli et al. 2000; Reisenegger et al. 2000; Einasto et al. 2003, 2007; Kaldare et al. 2003; Woudt et al. 2004; Fleenor et al. 2005, 2006; Proust et al. 2006; Radburn-Smith et al. 2006). However, a detailed large-scale mapping of all intervening structures (and the voids between them) with a purpose-built instrument has remained unavailable until now. The complementary 2MRS (Huchra et al. 2005) uses the 6dFGS in the south to provide an all-sky redshift survey of some 23 000 galaxies to $K = 11.25$ ($\bar{z} = 0.02$).

Figs 6 and 7 show the $z < 0.2$ Universe as seen by 6dFGS in the plane of the sky, projected in Galactic coordinates. The two figures show the Northern and Southern Galactic hemispheres, respectively. Familiar large-scale concentrations such as Shapley are obvious, and several of the key structures have been labelled. At $z < 0.02$, filamentary structures such as the Centaurus, Fornax and Sculptor walls (Fairall 1998) interconnect their namesake clusters in a manner typical of large structures generally. At $z \approx 0.006$ to 0.01 the Centaurus wall crosses the Galactic plane Zone of Avoidance (ZoA) and meets the Hydra wall at the Centaurus cluster. The Hydra wall then extends roughly parallel to the ZoA before separating into two distinct filaments at the adjacent Hydra/Antlia clusters, both of which extend into the ZoA. Behind these, at $z = 0.01$ to 0.02, a

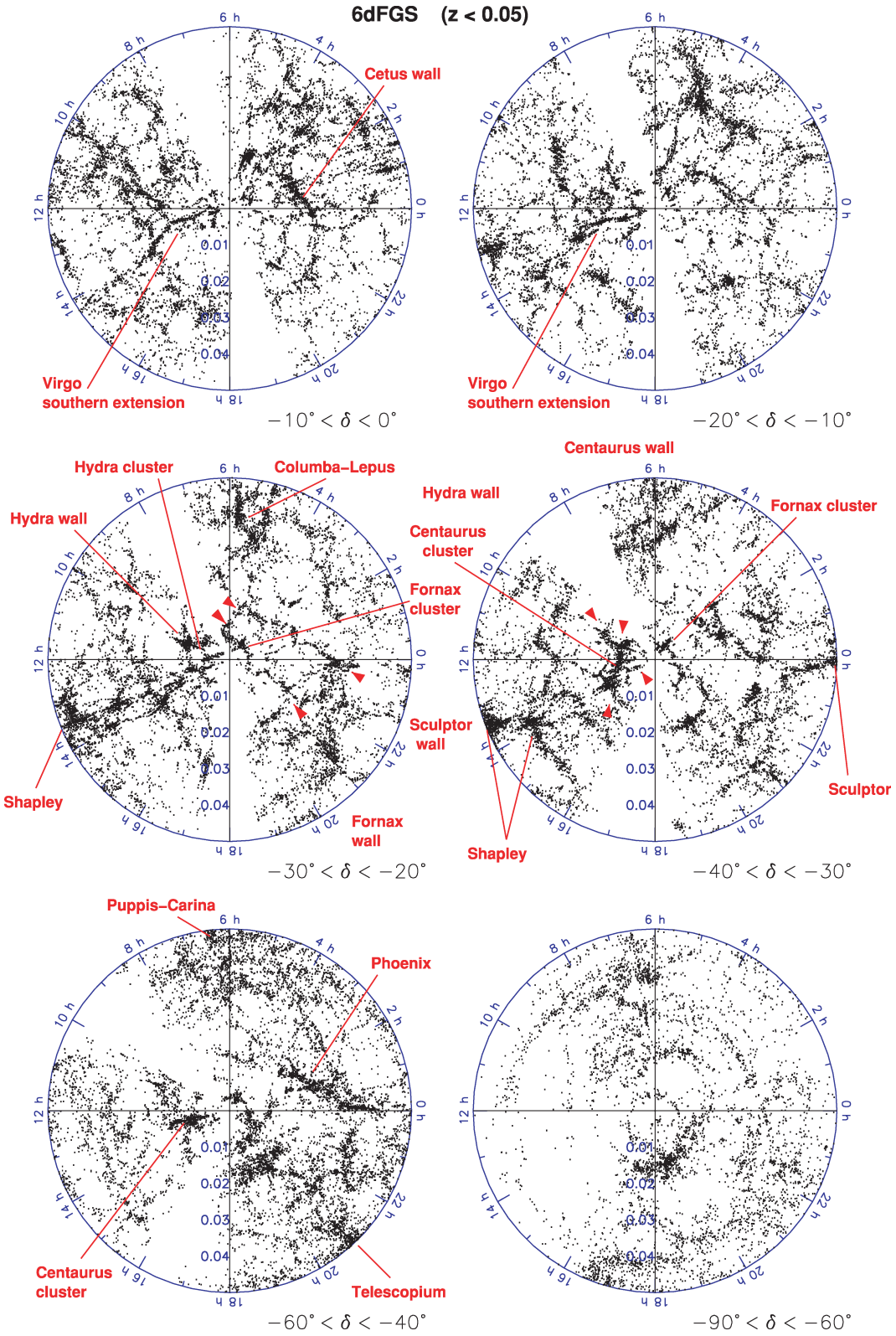

Figure 8. 6dFGS redshift maps out to $z = 0.05$, in Dec. slices of varying width from the equator to the pole.

separate filament incorporates the Norma and Centaurus-Crux clusters, and encompasses the putative Great Attractor region (Woudt et al. 2004; Radburn-Smith et al. 2006, and references therein). Beyond these, at $z = 0.04$ to 0.05, lies the Shapley supercluster complex, a massive concentration of clusters thought to be responsible for 10 per cent of the Local Group motion (Raychaudhury 1989; Bardelli et al. 2000; Reisenegger et al. 2000) or even more (Quintana et al. 1995; Drinkwater et al. 1999; Proust et al. 2006).

4.2 Declination slice projections

Figs 8 and 9 show an alternative projection of these structures, as conventional radial redshift maps, cross-sectioned in Dec. The two figures show the same data on two different scales, out to limiting redshifts of $z = 0.05$ and 0.1, respectively. The empty sectors in our maps correspond to the ZoA region.

Fig. 9 similarly displays the local Universe out to $z = 0.1$ with hitherto unseen detail and sky coverage. While Fig. 9 extends and confirms the now familiar labyrinth of filaments and voids (∼20

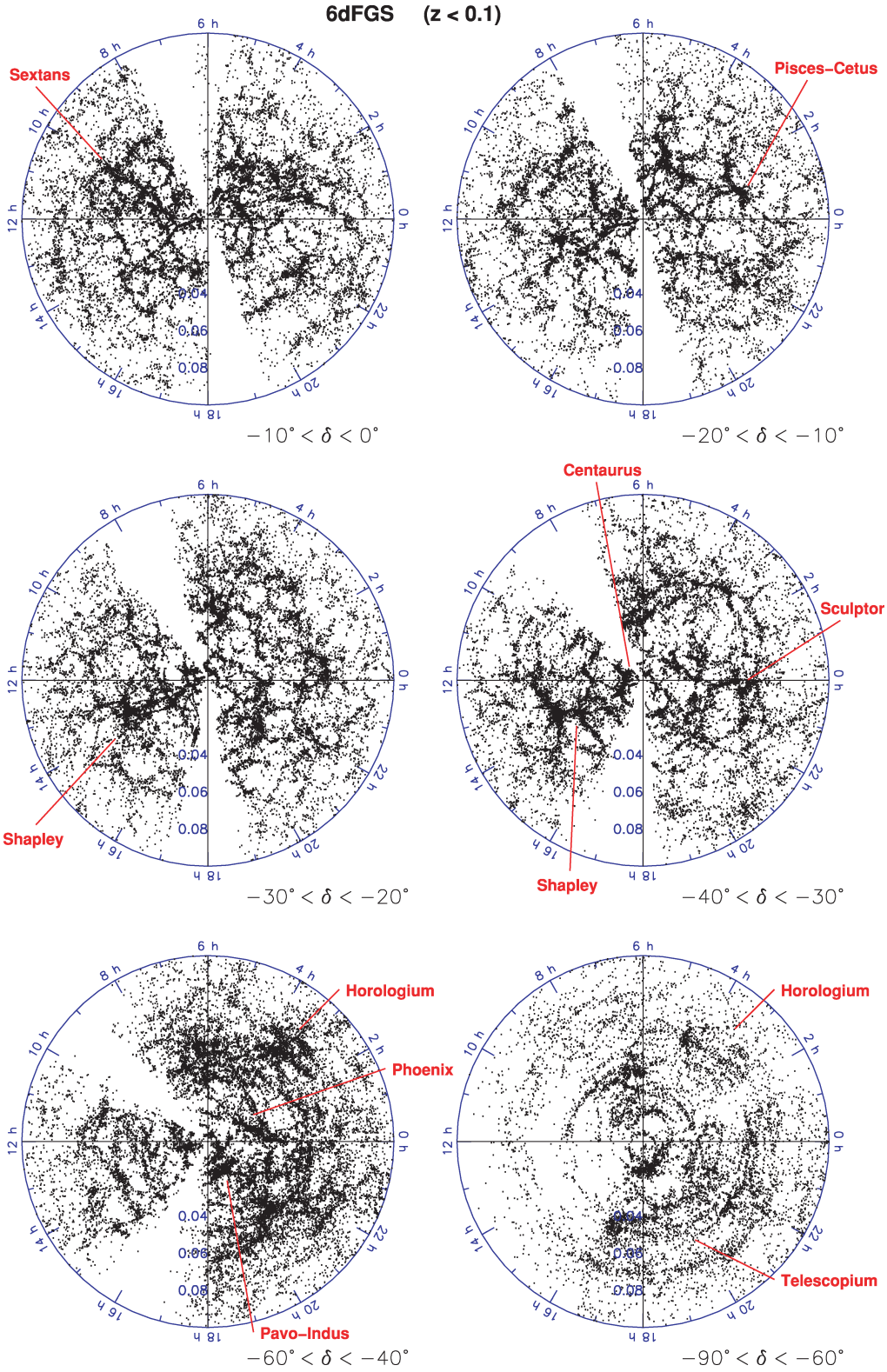

Figure 9. Same as Fig. 8, except on a larger scale out to $z = 0.1$.

to $40\,h^{-1}$ Mpc), it also reveals evidence of inhomogeneity on a still larger scales ($\gtrsim 60\,h^{-1}$ Mpc) – the plot for $-40^\circ < \delta < -30^\circ$ (middle right-hand panel) is a good example. A large underdense region at ($\Delta z \sim 0.02$ to 0.04) at $\alpha \approx 4$ to 5 h separates regions of compact high-density filaments; similar inhomogeneities are visible in the other plots. An extraordinarily large void ($\Delta z = 0.03$ to 0.06) is apparent in the plot for $-20^\circ < \delta < -10^\circ$, towards $\alpha \approx 23$ h. Other voids of this size are apparent when the data are examined in Cartesian coordinates. These voids are consistent with the shallower number counts observed in southern high-Galactic latitude regions compared to the north (e.g. Frith et al. 2003). The most extreme inhomogeneity, however, is the overdense Shapley region, which is unique within the sample volume (Einasto et al. 1997; Proust et al. 2006). Shapley has a sizable impact on the local peculiar velocity field (cf. Hudson et al. 1999, 2004).

Erdogdu et al. (2006b) have used spherical harmonics and Wiener filtering to decompose the density and velocity field of the shallower 2MRS. The correspondence between the largest scale superclusters and voids seen in both surveys at $z < 0.05$ is clear. Our southernmost projection ($-90^\circ < \delta < -60^\circ$) confirms the most distant (Pavo) of the three tentative superclusters of Fairall & Woudt (2006) while indicating that the other two are not major overdensities. We point out that this southern region is where 6dFGS coverage is generally lowest, with below-average completeness between 0 and 6 h and around the pole (poor sky coverage), and at 11 to 17 h (ZoA). Azimuthal stretching effects are also evident, due to the wide RA span of single fields at polar Dec.

Work is currently underway cataloguing new clusters and groups from 6dFGS using a percolation-inferred friends-of-friends algorithm (Huchra & Geller 1982; Eke et al. 2004). At the same time, a preliminary list of ∼500 void regions has been compiled as a reference for future work on underdense regions.

5 CONCLUSION

The 6dFGS is a combined redshift and peculiar velocity survey over most of the southern sky. Here we present the final redshift catalogue for the survey (version 1.0), consisting of 125 071 extragalactic redshifts over the whole southern sky with $|b| > 10^\circ$. Of these, 110 256 are new redshifts from 136 304 spectra obtained with the UKST between 2001 May and 2006 January. With a median redshift of $\tilde{z} = 0.053$, 6dFGS is the deepest hemispheric redshift survey to date. Redshifts and associated spectra are available through a fully searchable online SQL data base, interlinked with photometric and imaging data from the 2MASS XSC, SuperCOSMOS and a dozen other input catalogues. Peculiar velocities and distances for the brightest 10 per cent of the sample will be made available in a separate future release.

In this paper we have mapped the large-scale structures of the local ($z < 0.1$) southern universe in unprecedented detail. In addition to encompassing well-known superclusters such as Shapley and Hydra-Centaurus, the 6dFGS data reveal a wealth of new intervening structures. The greater depth and sampling density of 6dFGS compared to earlier surveys of equivalent sky coverage has confirmed hundreds of voids and furnished first redshifts for around 400 southern Abell clusters (Abell, Corwin & Olowin 1989).

The unprecedented combination of angular coverage and depth in 6dFGS offers the best chance yet to minimize systematics in the determination of the luminosity and stellar mass functions of low-redshift galaxies, both in the NIR and optical (e.g. Jones et al. 2006). While surveys containing $\sim 10^5$ galaxy redshifts (such as 6dFGS) have now reduced random errors to comparable levels of high precision, systematic errors remain the dominant source of the differences between surveys. For example, the evolutionary corrections that initially beset comparisons between 2dFGRS and SDSS (cf. Blanton et al. 2001; Norberg et al. 2002) are negligible for 6dFGS, which spans lookback times of only 0.2 to 0.7 Gyr across $[0.5\bar{z}, 1.5\bar{z}]$ (compared to 0.5 to 1.3 Gyr for SDSS and 2dFGRS). The minimization of such systematics is a feature of the 6dFGS luminosity functions (Jones et al. 2006).

In addition to these studies, 6dFGS redshift data have already been used to support a variety of extragalactic samples selected from across the electromagnetic spectrum. Deep H I surveys planned for next-generation radio telescopes (Blake et al. 2004; van Driel 2005; Rawlings 2006; Johnston et al. 2008) will also benefit from this redshift information as they probe the gas content of the local southern universe over comparable volumes.

ACKNOWLEDGMENTS

DHJ acknowledges support from Australian Research Council Discovery – Projects Grant (DP-0208876), administered by the Australian National University. JH acknowledges support from the US National Science Foundation under grant AST0406906. We also acknowledge the valuable contributions of an anonymous referee.

We dedicate this paper to two colleagues who made important contributions to the 6dFGS before their passing: John Dawe (1942–2004), observer and long-time proponent of wide-field fibre spectroscopy on the UKST from its earliest days, and Tony Fairall (1943–2008), whose unique insights from a career-long dedication to mapping the southern Universe underpin much of the interpretation contained herein.

REFERENCES

Abazajian K. et al. (the SDSS Collaboration), 2009, ApJS, 182, 543
Abell G. O., Corwin H. G. Jr., Olowin R. P., 1989, ApJS, 70, 1
Andernach H., Tago E., Einasto M., Einasto J., Jaaniste J., 2005, in Fairall A. P., Woudt P. A., eds, ASP Conf. Ser. Vol. 329, Nearby Large-Scale Structures and the Zone of Avoidance. Astron. Soc. Pac., San Francisco, p. 283
Bardelli S., Zucca E., Zamorani G., Moscardini L., Scaramella R., 2000, MNRAS, 312, 540
Baugh C. M., 2006, Rep. Prog. Phys., 69, 3101
Bell E. F., de Jong R. S., 2001, ApJ, 550, 212
Bell E. F., McIntosh D. H., Katz N., Weinberg M. D., 2003, ApJS, 149, 289
Bennett C. L. et al., 2003, ApJS, 148, 1
Bernardi M. et al. (SDSS team), 2003, AJ, 125, 1849
Blake C. A., Abdalla F. B., Bridle S. L., Rawlings S., 2004, New Astron. Rev., 48, 1063
Blanton M. R. et al. (SDSS team), 2001, AJ, 121, 2358
Boué G., Adami C., Durret F., Mamon G. A., Cayatte V., 2008, A&A, 479, 335
Branchini E. et al., 1999, MNRAS, 308, 1
Burkey D., Taylor A. N., 2004, MNRAS, 347, 255
Campbell L. A., 2009, PhD thesis, the Australian National University
Campbell L., Saunders W., Colless M., 2004, MNRAS, 350, 1467
Cole S. et al. (2dFGRS team), 2005, MNRAS, 362, 505
Colless M. et al. (2dFGRS team), 2001, MNRAS, 328, 1039
Drinkwater M. J., Proust D., Parker Q. A., Quintana H., Slezak E., 1999, Publ. Astron. Soc. Aust., 16, 113
Einasto M., Tago E., Jaaniste J., Einasto J., Andernach H., 1997, A&AS, 123, 119
Einasto M., Jaaniste J., Einasto J., Heinämäki P., Müller V., Tucker D. L., 2003, A&A, 405, 821
Einasto M. et al., 2007, A&A, 476, 697
Eke V. R. et al. (2dFGRS team), 2004, MNRAS, 348, 866

Erdogdu P. et al., 2006a, MNRAS, 368, 1515
Erdogdu P. et al., 2006b, MNRAS, 373, 45
Fairall A. P., 1998, Large-Scale Structures in the Universe. Wiley-Praxis, Chichester
Fairall A. P., Woudt P. A., 2006, MNRAS, 366, 267
Fleenor M. C., Rose J. A., Christiansen W. A., Hunstead R. W., Johnston-Hollitt M., Drinkwater M. J., Saunders W., 2005, AJ, 130, 957
Fleenor M. C., Rose J. A., Christiansen W. A., Johnston-Hollitt M., Hunstead R. W., Drinkwater M. J., Saunders W., 2006, AJ, 131, 1280
Fluke C. J., Barnes D. G., Jones N. T., 2009, Publ. Astron. Soc. Aust., 26, 37
Frith W. J., Busswell G. S., Fong R., Metcalfe N., Shanks T., 2003, MNRAS, 345, 1049
Hambly N. C. et al., 2001a, MNRAS, 326, 1279
Hambly N. C., Davenhall A. C., Irwin M. J., MacGillivray H. T., 2001b, MNRAS, 326, 1315
Huchra J. P., Geller M. J., 1982, ApJ, 257, 423
Huchra J. P., Geller M., Clemens C., Tokarz S., Michel A., 1992, Bull. CDS, 41, 31
Huchra J. et al., 2005, in Fairall A. P., Woudt P. A., eds, ASP Conf. Ser. Vol. 329, Nearby Large-Scale Structures and the Zone of Avoidance. Astron. Soc. Pac., San Francisco, p. 135
Hudson M. J., Smith R. J., Lucey J. R., Schlegel D. J., Davies R. L., 1999, ApJ, 512, L79
Hudson M. J., Smith R. J., Lucey J. R., Branchini E., 2004, MNRAS, 352, 61
Jarrett T. H., Chester T., Cutri R., Schneider S., Rosenberg J., Huchra J. P., Mader J., 2000, AJ, 120, 298
Johnston S. et al., 2008, Exp. Astron., 22, 151
Jones D. H. et al., 2004, MNRAS, 355, 747
Jones D. H., Saunders W., Read M., Colless M., 2005, Publ. Astron. Soc. Aust., 22, 277
Jones D. H., Peterson B. A., Colless M., Saunders W., 2006, MNRAS, 369, 25
Kaldare R., Colless M., Raychaudhury S., Peterson B. A., 2003, MNRAS, 339, 652
McIntosh D. H., Bell E. F., Weinberg M. D., Katz N., 2006, MNRAS, 373, 1321
Mahoney E. K., Croom S. M., Boyle B. J., Edge A. C., Sadler E. M., 2009, MNRAS, submitted
Mauch T., Sadler E. M., 2007, MNRAS, 375, 931
Mauduit J.-C., Mamon G. A., 2007, A&A, 475, 169
Norberg P. et al. (2dFGRS team), 2002, MNRAS, 336, 907
Parker Q. A., Watson F. G., Miziarski S., 1998, in Arribas S., Mediavilla E., Watson F., eds, ASP Conf. Ser. Vol. 152, Fiber Optics in Astronomy III. Astron. Soc. Pac., San Francisco, p. 80
Peacock J. A. et al., 2001, Nat, 410, 169
Percival W. J. et al., 2001, MNRAS, 327, 1297
Perlmutter S. et al., 1999, ApJ, 517, 565
Proust D. et al., 2006, A&A, 447, 133
Quintana H., Ramirez A., Melnick J., Raychaudhury S., Slezak E., 1995, AJ, 110, 463
Radburn-Smith D. J., Lucey J. R., Woudt P. A., Kraan-Korteweg R. C., Watson F. G., 2006, MNRAS, 369, 1131
Rawlings S., 2006, in Whitelock P., Dennefeld M., Leibundgut B., eds, IAU Symp. 232, The Scientific Requirements for Extremely Large Telescopes. Cambridge Univ. Press, Cambridge, p. 86
Raychaudhury S., 1989, Nat, 342, 251
Reisenegger A., Quintana H., Carrasco E. R., Maze J., 2000, AJ, 120, 523
Riess A. G. et al., 1998, AJ, 116, 1009
Sadler E. M. et al., 2007, MNRAS, 381, 211
Saunders W. et al., 2000, MNRAS, 317, 55
Schmidt B. P. et al., 1998, ApJ, 507, 46
Smith R. J., Lucey J. R., Hudson M. J., Schlegel D. J., Davies R. L., 2000, MNRAS, 313, 469
Smith R. J. et al., 2004, AJ, 128, 1558
Spergel D. N. et al., 2007, ApJS, 170, 377
van Driel W., 2005, in Casoli F., Contini T., Hameury J. M., Pagani L., eds, EDP-Sciences Conf. Ser., SF2A-2005 Semaine de l'Astrophysique Francaise. EDP Sciences, Les Vlis, p. 701
Watson F. G., Parker Q. A., Bogatu G., Farrell T. J., Hingley B. E., Miziarski S., 2000, Proc. SPIE, 4008, 123
Wegner G. et al., 2003, AJ, 126, 2268
Woudt P. A., Kraan-Korteweg R. C., Cayatte V., Balkowski C., Felenbok P., 2004, A&A, 415, 9
York D. G. et al. (SDSS team), 2000, AJ, 120, 1579
Zaroubi S., Branchini E., 2005, MNRAS, 357, 527

This paper has been typeset from a TEX/LATEX file prepared by the author.